Computer-Aided Design of Two-Dimensional Electric-Type Hyperthermia Applicators Using the Finite-Difference Time-Domain Method

Joseph A. Shaw, *Member, IEEE*, Carl H. Durney, *Senior Member, IEEE*, and Douglas A. Christensen, *Member, IEEE*

Abstract—**A hyperthermia applicator design tool consisting of a finite-difference time-domain (FDTD) technique in combination with a graphical display of electric fields and normalized linear temperature rise is described. This technique calculates, rather than assumes, antenna current distributions; it includes mutual interactions between the body and the applicator, and it calculates driving-point impedance and power delivered to the applicator. Results show that the fundamental limitation of 2-D electric-type applicators is overheating of the fat by normal components of the electric field, which exist because of near fields and capacitive coupling with the muscle. Two factors which contribute to the capacitance are the muscle conductivity and the small antenna size in air. Two examples of applicators designed to avoid fat overheating are described: a 27-MHz segmented dipole for heating large tumors to 7 cm depth, and a 100-MHz dipole for small tumors to 5 cm depth. The first uses a water bolus, and the second uses a water bolus with low-permittivity strips to reduce normal fields at the antenna ends. The results of this study describe fundamental limitations of electric field applicators, and illustrate the use of a powerful applicator design tool that allows rapid evaluation of a wide range of ideas for applicators which would require months and years to test experimentally.**

Introduction

During the last several years, there has been increasing interest in the application of numerical techniques to electromagnetic hyperthermia research [1]–[3]. Numerial techniques have been used to calculate the electric fields and resulting specific absorption rate (SAR) in man models with plane-wave illumination [4], and to calculate the electric fields in models of the body with existing applicators [2], [5]. Although numerical techniques have been used for applicator design with homogeneous tissue models [6], and as a tool in analyzing antennas for interstitial hyperthermia [7], they apparently have not been widely used to design noninvasive hyperthermia applicators with heterogeneous tissue models.

Manuscript received November 20, 1989; revised November 16, 1990. This work was supported by National Institutes of Health Grant P01 Ca 29578-07.

The authors are with the Departments of Electrical Engineering and Bioengineering, University of Utah, Salt Lake City, UT 84112.

IEEE Log Number 9101996.

In this paper, we describe a study of the fundamental limitations of 2-D (two-dimensional) electric-(E-) field type applicators with heterogeneous tissue distributions, using the finite-difference time-domain (FDTD) technique configured as a hyperthermia applicator design tool. This design tool allows the designer to investigate ideas much more rapidly than could be done experimentally.

We first describe the technique and then identify and explain the fundamental limitation of E-field applicators, including an unsuspected capacitive-coupling mode found in some electric dipole configurations. Following this, we summarize the results of a numerical study of E-field applicators; in doing so, we demonstrate the utility of the FDTD technique as an applicator design tool.

FDTD Technique for Applicator Design

The FDTD technique is well suited to hyperthermia calculations because of its capability of modeling heterogeneous electromagnetic problems and its conservative demand for computational resources (relative to integral techniques) [3], [8]. New models are generated quite easily with simple alterations of an input file; this provides a convenient, user-friendly interface between the user and the program.

We used a standard FDTD algorithm [8], which is an alternate space-time, centered-difference approximation of the Maxwell curl equations on a discretized grid. The grid consists of square cells, with each cell defined by the permittivity and conductivity of the material it represents. The values we use for these dielectric parameters are listed in Table I [9].

Our 2-D program positions the grid in an x-y plane, and includes field components E_x, E_y, and H_z. Fig. 1 indicates how the field components are defined on a standard Yee cell [8], with E fields on the edges of each cell, and the H field at the center of the cell. This arrangement correctly simulates Maxwell's equations for each cell. Dielectric interfaces lie along cell edges, and we have found that permittivity averaging at these interfaces is important for the stability and symmetry of the solution. The user defines the source with either an H-field or E-field com-

TABLE I
DIELECTRIC PARAMETERS USED IN FDTD MODELS [9]

27 MHz	ϵ_r	σ(S/m)
fat	20.0	0.027
muscle	113.0	0.612
40 MHz	ϵ_r	σ(S/m)
fat	14.6	0.033
muscle	97.3	0.693
100 MHz	ϵ_r	σ(S/m)
fat	7.45	0.0475
muscle	71.7	0.889

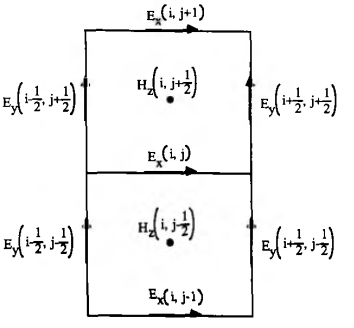

Fig. 1. Field components in the 2-D FDTD model.

ponent. For example, we define our 2-D dipole models to be two infinitely wide sheets of copper separated by an airgap; we then specify the magnitude (e.g., 100 V/m) and phase of an E-field component across the airgap, with the E field polarized along the dipole axis. The program initializes all nonsource field components to zero, and alternately calculates magnetic and electric fields throughout the grid from the discretized Maxwell curl equations. The program repeats this process, at time increments equal to one-half the cell size divided by the free-space wave velocity, for a user-specified number of cycles of the source field (usually three cycles in our models). The length of time that calculations must continue is dictated by the time required for the transient solution to decay, and for the steady-state solution to appear.

This method removes uncertainties due to assumed antenna current distributions because all electromagnetic effects, such as scattering, diffraction, and antenna end effects are inherent in the Maxwell curl equations. In fact, we have used this program to calculate the current distribution on applicators from the H-field components along the antenna edges, and have obtained useful information about applicator-to-body coupling mechanisms.

An important element of our FDTD design tool is graphical display of the E fields, SAR's and heating patterns. By examining both the E field and heating patterns for several design variations, much can be learned about the relationships among applicator shape and size, applicator placement relative to the body, bolus arrangements, and heating capability. We usually look at plots of the steady-state E field at two different instants of time: at the beginning of a steady-state cycle ($t = 0$), and a quarter cycle later ($T = T/4$) where $t = 0$ is with reference to the steady-state sinusoidal voltage source and T is the period of the sinusoidal voltage source. E-field pictures at two instants of time are often needed to get a clear picture of how the normal E-field components overheat the fat, since at particular instants of time these important components may be relatively small. Because of the repetitive nature of the field pattern, the patterns at two instants of time are usually enough to get good understanding about the basic nature of the fields. To save space, in this paper we have shown the fields at only the most informative instant of time.

Fig. 2 is an example of an electric field plot from this technique; the lines are in the direction of the E field and their lengths are proportional to the field strength in each cell. A circle at the end of a line indicates a vector tail. Each E-field vector is the vector sum of E_x and E_y for each cell at the cell center. A small dot at the cell center indicates that the vector at that point is too small to represent by a line length. Fig. 2 illustrates the E field for a 2-D half-wave dipole in free space, which agrees qualitatively with the analytical solution for a wire dipole. Comparison of FDTD results with those obtained by analytical solution of a parallel-plate waveguide verify the accuracy of the technique.

From the E fields calculated by the FDTD program, we calculate the SAR from SAR $= \sigma E^2/\rho$ where σ is the conductivity, E^2 is the square of the rms sinusoidal steady-state electric field, and ρ is the mass density. We also calculate the linear temperature rise T_r from $T_r =$ SAR$/C_p$, in degrees/second where C_p is the specific heat. Then we normalize T_r to the maximum value that occurs anywhere in the model. This normalized linear temperature rise is the temperature rise that occurs when the heating is fast enough that the temperature rise is linear with respect to time; i.e., the heating is fast enough that thermal diffusion is negligible. For muscle we used $C_p\rho = 4.178\ (10^6)$ Joules/°C m^3, and for fat, $C_p\rho = 1.863\ (10^6)$ Joules/°C m^3 [10].

The FDTD technique has disadvantages as well, some of which are not serious for hyperthermia modeling. For example, the grid must be truncated in space with absorbing boundary conditions that simulate outgoing waves radiating to infinity, with no reflection [11]. Our program uses the Mur first-order boundary conditions described in [11]. These boundaries, if not placed far enough away from an antenna that outgoing waves are at near-normal incidence, can produce serious errors due to nonphysical reflections interfering with the computations near the center of the grid. (By nonphysical reflections, we mean those produced mathematically by the imperfect boundary con-

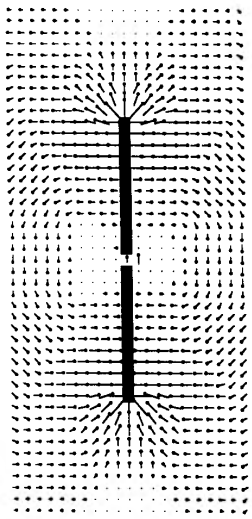

Fig. 2. Steady-state electric field at $t = T/4$ (referenced to the sine-wave electric field source) for a half-wave dipole in free space.

ditions.) However, for hyperthermia models, the abundant lossy tissue helps absorb both outgoing waves before they reach the boundaries, and nonphysical reflections before they can interfere with central-grid computations. Thus, grid truncation is not as serious an issue for hyperthermia modeling as it is for free-space scattering. Also, the graphical display of E fields removes much of the uncertainty of boundary condition accuracy. If the boundaries cause the field solutions to degrade significantly, it is usually recognizable as asymmetric, or otherwise unexpected patterns in the E-field plots.

The model used to create Fig. 2 is typical of those used throughout this study. The cell size is 1 cm, in this case chosen to allow resolution of the physical features of interest, although often the cell size is chosen to ensure adequate spatial sampling (at least ten cells per wavelength). The computational domain is roughly three times as large as that shown in Fig. 2, to allow the dipole fields to become nearly planar before intersecting the computational boundary. In the models with lossy tissue, the computational domain is usually between 20 and 50% larger than shown, thanks to the damping afforded by the lossy tissue.

Since single-cell layers are not adequate for rapidly varying spatial fields, we checked our results for single-cell layers with those with reduced cell size, and where required used these increased-resolution models. For most of the cases described here, single-cell layers were adequate.

Although the 2-D study is useful for identifying the fundamental behavior and limitations of some applicators, particulary electric-dipole applicators, 3-D models are needed to optimize actual applicator design. It is more efficient, though, to learn as much as possible and solve some of the fundamental problems using the simpler and less expensive 2-D design tool than to try and use the more complicated and expensive 3-D models from the beginning.

In what follows, we describe some fundamental characteristics of 2-D models of electric dipoles. Since these 2-D dipoles are infinitely wide, we refer to them as sheet dipoles. In some cases, these 2-D dipole models would be good approximations to actual sheet dipoles consisting of two thin metallic sheets separated by a gap.

Fundamental Limitations of E-Field Applicators

This paper indicates that overheating of the fat by the normal E components fundamentally limits deep-heating of heterogeneous tissue with this class of applicators. There are two contributing causes of normal E fields: 1) capacitive-like coupling of the antenna with the muscle tissue, and 2) intersection of the fat layer by near fields of the antenna. Although these two causes are both near-field effects, we have differentiated them because the capacitive-like coupling is such an extreme and characteristic form of near-field behavior that it is important to describe it separately. As far as we know, this capacitive-like coupling (described in detail below) has not been discussed in the literature.

As is well known [12], fat is overheated by normal E-field components at the fat–muscle interface because, by boundary conditions, the ratio of normal-field magnitudes in the two media is equal to the inverse ratio of permittivities, i.e., letting the subscripts f and m denote fat and muscle, respectively:

$$\frac{E_f}{E_m} = \frac{\epsilon_m}{\epsilon_f} \tag{1}$$

at the boundary, where E_f and E_m are normal E fields. Because the permittivity of muscle is much higher than that of fat, a normal electric field in fat is much higher than that in the muscle. The power absorbed in the tissue is proportional to σE^2 where σ is conductivity. Thus, even though the conductivity is higher for muscle than fat, E^2 dominates and the power absorbed in the fat is typically several times that in muscle. For example, at 27 MHz the SAR in the fat is roughly eight times that in the muscle for normal E-field polarization [12]. However, a tangential electric field is continuous across the dielectric interface. Therefore, the lower fat conductivity results in lower power deposition in the fat than in the muscle for a tangential E field. Thus, for heating muscle tissue without overheating the fat, the electric field should be mostly tangential at the fat–muscle interface.

With our FDTD technique, we have found that a sheet dipole that is resonant size in muscle (i.e., with length equal to one-half wavelength in muscle) can couple to the body in a perhaps unsuspected, but easily understood, capacitive-like mode if spaced from the body by a small thickness of dielectric. This capacitive-like coupling can be explained with reference first to Fig. 3, which shows that a half-muscle-wavelength dipole directly against a homogeneous muscle region radiates preferentially into

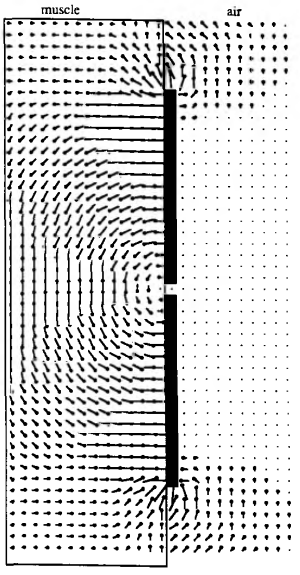

Fig. 3. Electric field at $t = T/4$ (referenced to the sine-wave electric field source) for a 27 MHz half-wavelength (in muscle) dipole directly against a muscle mass.

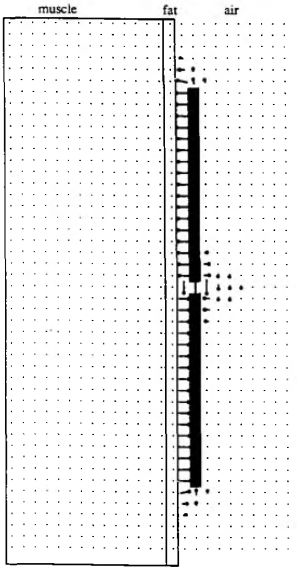

Fig. 4. Electric field at $t = 0$ (referenced to the sine-wave electric field source) for a 27 MHz half-wavelength (in muscle) dipole, separated by a 1-cm air gap from a 1-cm fat layer over muscle. The uniform normal fields are due to capacitive coupling of the dipole with the muscle.

the muscle, presumably because the antenna is of resonant size in the muscle and electrically small in air.

The addition of a 1-cm fat layer and a 1-cm air gap to the muscle results in a much different electric-field pattern, as shown in Fig. 4: the fields are essentially uniform along the antenna (as compared to the varying fields in the case shown in Fig. 3), and normal to the interface, as in a parallel-plate capacitor. Fringing of the fields at the

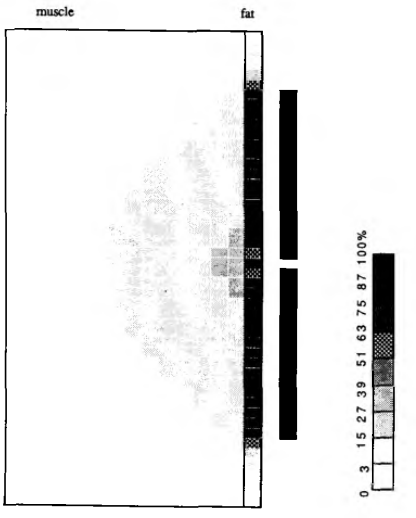

Fig. 5. Normalized linear temperature rise pattern for the configuration of Fig. 4. In the tissue, black represents maximum temperature rise and white minimum temperature rise.

ends of the antenna similar to that for a parallel-plate capacitor can also be seen in the plot, but the 1-cm cells are too large to show the fringing pattern in detail. The strong normal fields produce the normalized linear temperature rise pattern of Fig. 5, with severe fat heating along the entire length of the antenna. This capacitive mode is actually the combination of two effects: 1) the half-muscle-wavelength dipole is electrically small in the air gap, and 2) the dipole forms a parallel-plate capacitor with the fairly high-conductivity muscle acting like an opposing plate. An electrically small dipole in air with no tissue present is essentially equivalent to a capacitance. When the tissue is present, this capacitive effect is increased because the muscle acts like another metal plate, which increases the capacitive coupling.

Fig. 6 illustrates this capacitance behavior with a plot of the current density along the antenna of Fig. 4, compared with that of the dipole with length slightly greater than one-half a free-space wavelength; both current density plots were obtained from FDTD data. Note that the free-space dipole exhibits a current density that is sinusoidal, but with a small dip at the antenna center, as is expected for a 0.52-wavelength dipole [13]. However, the antenna of Fig. 4 has a linear current distribution. The linear current distribution implies capacitive behavior because from the current continuity equation, $\nabla \cdot \boldsymbol{J} = -\partial\rho/\partial t$ where $\boldsymbol{J}$ is current density and ρ is charge density, and when $\boldsymbol{J}$ is linear along the antenna surface, ρ is constant along the surface. Since the normal component of $\boldsymbol{E}$ at the surface is equal to the surface charge density, a constant surface charge density means a constant $\boldsymbol{E}$, as in a capacitor. It is surprising that the half-muscle-wavelength dipole acts so much like a capacitor when the air gap and fat layer are so small compared to a wavelength. One might have expected that such an electrically small

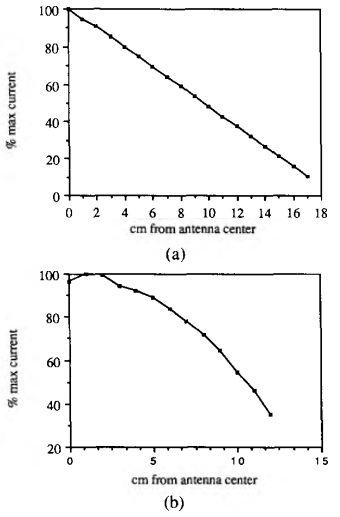

Fig. 6. Current distribution for (a) 27 MHz capacitive half-wavelength (in muscle) dipole separated from muscle by 1 cm of fat and 1 cm of air (Fig. 4) and (b) 600 MHz radiative half-wavelength dipole in free space (Fig. 2).

gap would have a small effect on the radiation into the muscle. This analysis illustrates some of the advantages of the FDTD method in obtaining information useful in applicator design. Serious errors would have resulted from assuming a typical sinusoidal current distribution along the dipole of Fig. 4.

We have investigated several variations of the configuration in Fig. 4 to verify that there are actually two factors contributing to the capacitive coupling, each of which can exist essentially independently of the other. These variations include replacing the muscle in Fig. 4 with a metal sheet to verify that the muscle is acting like a conducting layer; lengthening the dipole to a half-wavelength in free space so it is not electrically small; and placing the half-muscle-wavelength dipole directly against the fat to eliminate the effect of the air gap. In the latter two models, less capacitive-like coupling occurred than that of Fig. 4; however, capacitive-like coupling still dominated. Thus, there does appear to be the two nearly independent components of capacitive coupling, the electrical shortness of the antenna in air, and the effect of the muscle similar to that of another capacitor plate. The FDTD data for these examples show that removal of either component is accompanied by a departure from perfectly linear current distribution to a slightly curved, but by no means sinusoidal, current distribution along the antenna.

Since the normal components of E are basically characteristic of the near fields, another way to look at the capacitive coupling is that it increases the near-field normal components dramatically. Near fields are a general problem with hyperthermia applicators because their strong normal components overheat the fat, and also because they decay rapidly with increasing distance from the antenna, so do not contribute much to heating at depth relative to the heating at the surface.

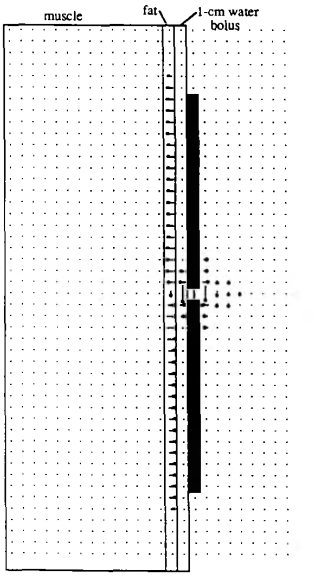

Fig. 7. Electric field at $t = T/4$ (referenced to the sine-wave electric field source) for a 27 MHz half-wavelength (in muscle) dipole, separated by a 1-cm water bolus from fat and muscle.

Fig. 7 shows an electrical field pattern for a configuration similar to Fig. 4, but with the air gap replaced by a water bolus; Fig. 8 is the corresponding normalized linear temperature rise pattern. The water bolus reduces the capacitive-like coupling, but the remaining near-fields are still a problem. In Fig. 5, the stronger capacitive coupling distributes the high fat temperature rises along each half of the dipole whereas the maximum temperature rise occurs directly under the feed point in Fig. 8.

FDTD-Based Design for Reducing Normal Fields

Far-Field-Thick Boluses

As indicated by Fig. 8, a water bolus can reduce the near-field normal components and lessen the heating in the fat. As the water bolus is made thicker, the hot spots in the fat appear to move away from the feed point toward the dipole ends, until eventually near fields no longer intersect the fat, and radiative coupling is achieved. At this point, only far fields (radiative fields) intersect the fat. We call a bolus that produces these conditions a far-field-thick bolus. These fields are primarily tangential to the fat, and thus heat the muscle more than the fat. For radiative coupling, the SAR is maximum at the near boundary of the muscle region, and attenuates with increased depth in the tissue. An array of radiative applicators has been shown to produce equal, maximum SAR at the center and outer edge of a cylindrical muscle region, with a minimum in between [5].

In planar nontissue models in which the permittivity does not depend on frequency, we have found that a rough estimate of the thickness r of a water bolus required for far-field coupling can be obtained by requiring $kr = 4.5$

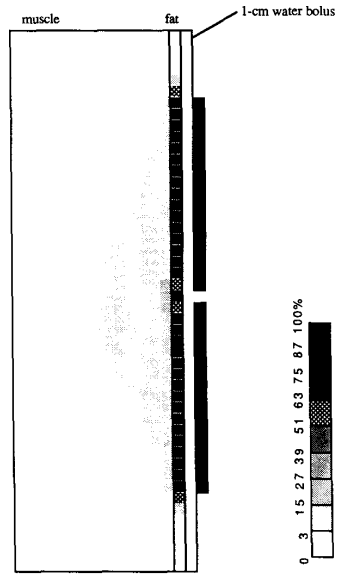

Fig. 8. Normalized linear temperature rise pattern for the configuration of Fig. 7.

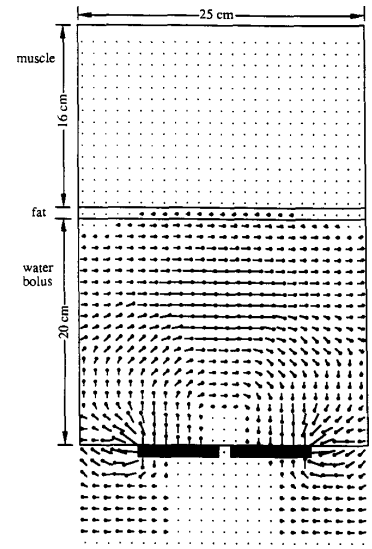

Fig. 9. Electric field at $t = T/4$ (referenced to the sine-wave electric field source) for a 100 MHz half-wavelength (in muscle) dipole with a 20 cm water bolus. The far-field thick bolus allows this applicator to couple radiatively with the body, producing maximum linear temperature rise in the muscle rather than in the fat (see Fig. 10).

where k is the propagation constant constant in the bolus. In tissue models, however, the frequency-dependence of fat permittivity has a large effect on the required thickness of the bolus because the ratio of water bolus permittivity to fat permittivity, for example, is approximately 4 at 27 MHz, 6 at 40 MHz, and 12 at 100 MHz. The larger permittivity discontinuity at the bolus–fat interface for the higher frequencies means that very small normal E-field components in the bolus will result in very large normal components in the fat. Because of this, we have found that the bolus thickness required for maintaining the maximum fat heating at less than about 80% of the maximum muscle heating at the three frequencies mentioned does not scale in proportion to the frequency. For example, the bolus thickness required at 27 MHz was found to be about 44 cm, whereas our empirical rule for nontissue models predicts a thickness of between 50 and 60 cm. The required bolus thickness at 40 MHz is 40 cm, nearly the same as for 27 MHz, and at 100 MHz a 20-cm water bolus was sufficient. Since a 40-cm water bolus would be heavy and extremely inconvenient to use, 27 and 40 MHz dipoles may not be practical.

Fig. 9 shows the electric field for a half-muscle-wavelength dipole at 100 MHz, with a 20-cm water bolus. The fields intersect the fat mostly tangentially, and therefore produce a normalized linear temperature rise pattern that is maximum in the muscle, as shown in Fig. 10. To compare the penetration of the dipole fields with planewave penetration we made some additional calculations. First, we used the FDTD program to calculate the Poynting vector of a planewave incident on a planar homogeneous muscle model. The planewave depth of penentration (e^{-2} power point) from these calculations agreed with the

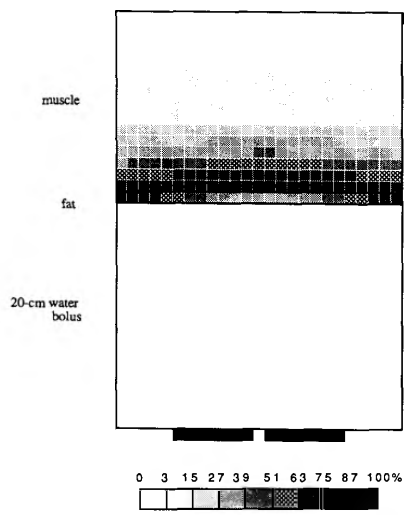

Fig. 10. Normalized linear temperature rise for the configuration of Fig. 9.

planewave depth of penetration given in [9]. Then we doubled the resolution (1/2-cm cells) and calculated the Poynting vector for the fat–muscle model of Figs. 9 and 10, first for planewave fields and then for the 100-MHz dipole fields. Since temperature rise is the desired end point in hyperthermia, for the fat–muscle model we compared the depths at which the normalized linear temperature rise in the muscle is one-half that at the front surface of the fat. This depth is much less than the e^{-2} power

point, of course, but is has more meaning with regard to heating tumors. The half-temperature-rise point for the planewave was about 2.8 cm from the fat front surface compared to 2.5 cm for the dipole fields. Thus with a far-field-thick water bolus, the half-wavelength 100-MHz dipole produces almost as much penetration as a planewave.

Other Bolus Arrangements

We then studied other variations of the applicator/bolus arrangement and found that each has potential problems: 1) an air gap between the antenna and a far-field-thick water bolus produces strong capacitive-like coupling, once again overheating the fat with strong normal fields near the ends of the dipole; 2) air gaps between the bolus and the body distort the tangential E field, once again causing normal E-field components at the fat layer, and, 3) tapering the bolus toward the body to a width less than the dipole length also distorts the fields and causes hot spots in the fat at the bolus edges.

While investigating ways of reducing normal fields with bolus variations, we found that normal E-field components can be reduced by inserting air strips into the bolus, because of the large discontinuity in permittivity at the air–water interfaces. To illustrate the idea, consider simple models of ideal capacitors with layers of water and air between the plates as shown in Fig. 11. The electric field in the air in the ideal capacitor of Fig. 11(a) is given by

$$E = \frac{V/d}{3 + 2\epsilon_a/\epsilon_w} \tag{2}$$

where ϵ_a and ϵ_w are the relative permittivities of air and water, respectively, V is the applied potential difference, and d is the thickness of each water layer and each air layer. Assuming for convenience that the relative permittivity of water is about 100 times that of air gives

$$E = \frac{V/d}{3.02}. \tag{3}$$

For the same conditions, the electric field in the air for the capacitor of Fig. 11(b) is given by

$$E = \frac{V/d}{1.04}. \tag{4}$$

Thus, the normal electric field in the air is substantially less in the capacitor with alternating layers of air and water than in the capacitor with only a single layer of air and a thicker layer of water. This result infers that alternating layers of air in a water bolus might reduce the normal component in the fat for a given thickness of water bolus.

It turned out that this type of bolus did indeed reduce the bolus thickness required for the dipoles; however, the dipoles coupled to this bolus with a much higher capacitive reactance than before, and also did not preferentially radiate into the bolus as well. The predicted temperature rise in the tissue for this configuration with the same source voltage as the previous cases is much too small to be practical. A variation of this bolus does, however, seem

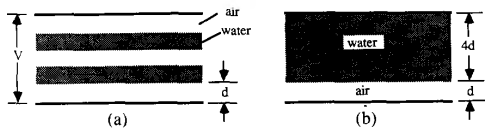

Fig. 11. (a) Ideal parallel-plate capacitor with alternating layers of air and water. (b) Ideal parallel-plate capacitor with one thick layer of water and one thin layer of air.

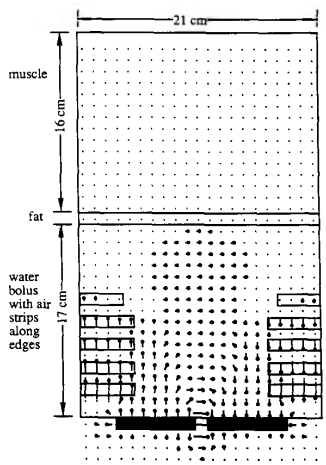

Fig. 12. Electric field at $t = 0$ (referenced to the sine-wave electric field source) for a 100-MHz half-wavelength (in muscle) dipole with a 17-cm water bolus with air strips near the dipole ends. The air strips at the dipole edges allow a 20% reduction in bolus thickness.

useful. By placing the air strips in the water bolus only near the dipole ends, where the limiting near-field normal components exist, the tangential fields from the center of the antenna are affected very little. This results in a much improved coupling, and does in fact reduce the bolus thickness required for the 100-MHz dipole from 20 to 17 cm, a 20% reduction in bolus thickness. Fig. 12 shows the E field for this design, and Fig. 13 shows the corresponding normalized linear temperature rise pattern. This single 15-cm long applicator might heat small tumors at 4–5 cm depth, and an array of such applicators might heat at still greater depth.

Alternate Antenna Designs

Another design that appears to be useful, especially for large tumors, is a 27-MHz half-muscle-wavelength dipole that is divided into segments, as shown in Fig. 14. The applicator is fed at each gap, with a voltage at each gap that corresponds to a sinusoidal distribution along the antenna with a maximum at the center, and all the voltages in phase. This feed distribution forces a sinusoidal current distribution as is expected for a radiating half-wave dipole. For this segmented dipole, the normal E-field components at each gap tend to cancel with those of the adjacent gap; the result is an overall reduction of normal E fields so that we can now use a 25-cm bolus instead of the 44-cm bolus that was required at 27 MHz for the unseg-

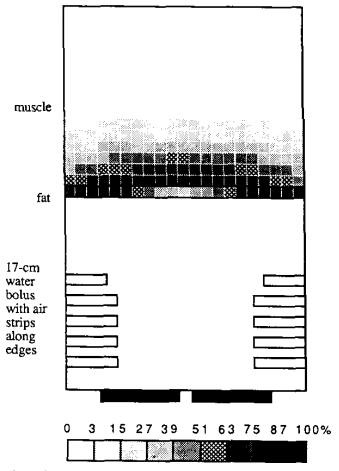

Fig. 13. Normalized linear temperature rise for configuration of Fig. 12.

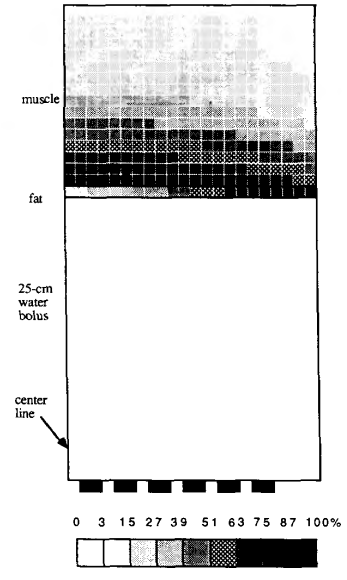

Fig. 14. Normalized linear temperature rise for segmented 27-MHz half-wavelength (in muscle) dipole with a 25-cm water bolus and a sinusoidal feed distribution (note that only half the antenna is shown). The required bolus thickness is reduced from 44 to 25 cm, presumably because the normal E fields for each gap tend to cancel with those of adjacent gaps.

mented straight dipole. The normalized linear temperature rise pattern in Fig. 14 shows that this applicator provides 7 cm penetration over a fairly large area (10–20 cm wide). Thus, this applicator might be useful for relatively large tumors. It is interesting to note that at 100-MHz the segmented dipole did not achieve much improvement over the straight dipole; similarly, air strips at the edge of the bolus with the segmented 27-MHz dipole did not make any significant difference. The frequency variation in fat-to-water permittivity ratio mentioned previously seems to be the main cause of some configurations working better at one frequency than another. We verified this theory by repeating the aforementioned calculations with the frequency-dependence of fat permittivity removed.

Limitations of 2-D Models

Several ideas that we would like to try cannot be adequately modeled with a 2-D program. For example, by folding the dipole ends back around to form a return path, thereby eliminating the pile-up of charges that occurs at the ends of the dipole, we hoped to reduce the normal E fields at the ends of the applicator. The resulting applicator (essentially a folded dipole) operates with two modes: a transmission-line mode, wherein the charges circulate around the loop; and an antenna mode, wherein the charges oscillate back and forth along the dipole. Unfortunately, because the transmission-line mode creates a magnetic field that circulates around the conductor, our 2-D model with only one magnetic-field component can not model this applicator. Indeed, 2-D models of an inductively fed metal loop in the x-y plane showed a z component of magnetic field inside the loop and zero fields outside the loop. In other words, a loop in the 2-D model seems to be like an infintely long solenoid with no external fields. Thus, a 3-D program is needed for modeling closed loops of finite length. We now have a 3-D program in the final stages of development, and calculations using it verify these conclusions about closed loops. Applicator design based on this 3-D program will be reported later.

Discussion

The FDTD technique is well suited to modeling hyperthermia applicators. Coupled with graphical display of the E fields and normalized linear temperature rises, and calculations of input impedance, antenna current, and input power, it provides a designer with enough information that applicator ideas can be rapidly tested and improved. With this tool many ideas can be tested in a short amount of time, and ideas which do not work can be discarded before lengthy experimental work is invested in them. This tool cannot replace experimental work, or course, but it can provide important insight into various relationships between an applicator's size, shape, placement relative to the body, and power deposition in human tissue. This insight can be used to design better applicators and avoid lengthy experimental testing of designs that do not work.

This study has shown that the fundamental limitation of E-field applicators is fat overheating by normal components of the electric field. These normal components are due to two phenomena: 1) capacitive coupling of the applicator with the tissue, and 2) intersection of fat by antenna near fields. Recognizing that a sheet dipole close to the body can behave like a parallel-plate capacitor, rather than like a radiator, is important to understand when attempting to optimize E-field applicators. Furthermore, realizing that a radiating antenna must be separated by a far-field-thick bolus to avoid near-field heating of the fat is also important. Both of these ideas show the importance of including a fat layer in models for numerical or exper-

imental applicator testing. Ignoring the fat is ignoring the fundamental limitation of this type of applicator.

It should be noted that all of these results are strictly valid only for sheet-type applicators, as opposed to wire antennas. Although wire antennas most likely share the same type of fundamental limitations as described in this paper, it could be that the 2-D nature of our solution enhances the capacitance beyond that found in actual wire antennas. Therefore, these results should only be interpreted directly for sheet-type applicators, and care should be exercised in applying them to wire antennas.

We have used our 2-D FDTD applicator design technique to design two applicators that appear worth testing experimentally: a 36-cm long 27-MHz segmented dipole with a 25-cm thick water bolus, and a 15-cm long 100-MHz dipole with a 17-cm thick water bolus that incorporates air strips near the dipole ends to reduce normal E fields. The 27-MHz applicator would be useful for heating relatively large tumors at depths at 7 cm, while the 100-MHz applicator would be best suited for small tumors at 4–5 cm depth, and could be implemented in an array.

Further work is needed to refine the FDTD applicator design technique, particularly in developing capability for 3-D calculations. Initial results from our 3-D code show that it promises to provide important new design capability for electromagnetic hyperthermia applicators.

Acknowledgment

We thank the reviewers for their helpful comments.

References

[1] J. W. Strohbehn and R. B. Roemer, "A survey of computer simulations of hyperthermia treatments," *IEEE Trans. Biomed. Eng.*, vol. BME-31, pp. 136–149, 1984.

[2] K. D. Paulsen, J. W. Strohbehn, and D. R. Lynch, "Theoretical electric field distributions produced by three types of regional hyperthermia devices in a three-dimensional model of man," *IEEE Trans. Biomed. Eng.*, vol. BME-35, pp. 36–44, 1988.

[3] D. M. Sullivan, D. T. Borup, and O. P. Gandhi, "Use of the FDTD method in calculating EM absorption in human tissues," *IEEE Trans. Biomed. Eng.*, vol. BME-34, pp. 148–157, 1987.

[4] D. M. Sullivan, O. P. Gandhi, and A. Taflove, "Use of the FDTD method for calculating EM absorption in man models," *IEEE Trans. Biomed. Eng.*, vol. BME-35, pp. 179–186, 1988.

[5] C. Q. Wang and O. P. Gandhi, "Numerical simulation of annular-phased arrays for anatomically based models using the FDTD method," *IEEE Trans. Microwave Theory Tech.*, vol. MTT-37, pp. 118–126, 1988.

[6] R. W. M. Lau, R. J. Sheppard, G. Howard, and N. M. Bleehen, "The modeling of biological systems in three dimensions using the time-domain finite-difference method: II. The application and experimental evaluation of the method in hyperthermia applicator design," *Phys. Med. Biol.*, vol. 31, pp. 1257–1266, 1986.

[7] M. F. Iskander and A. M. Tumeh, "Design optimization of interstitial antennas," *IEEE Trans. Biomed. Eng.*, vol. BME-36, pp. 238–246, 1989.

[8] A. Taflove and K. R. Umashankar, "The finite-difference time-domain (FDTD) method for electromagnetic scattering and interaction problems," *J. EM Waves Appl.*, vol. 1, no. 3, pp. 243–267, 1987.

[9] C. C. Johnson and A. W. Guy, "Nonionizing electromagnetic wave effects in biological materials and systems," *Proc. IEEE*, vol. 60, pp. 692–718, 1972.

[10] R. C. Gordon, R. B. Roemer, and S. M. Horvath, "A mathematical model of the human temperature regulatory system—Transient cold exposure response," *IEEE Trans. Biomed. Eng.*, vol. BME-23, pp. 434–444, 1976.

[11] J. G. Blaschak and G. A. Kriegsman, "A comparative study of absorbing boundary conditions," *J. Comp. Phys.*, vol. 77, pp. 109–139, 1988.

[12] D. A. Christensen and C. H. Durney, "Hyperthermia production for cancer therapy: A review of fundamentals and methods," *J. Microwave Power*, vol. 16, no. 2, pp. 89–105, 1981.

[13] C. A. Balanis, *Antenna Theory—Analysis and Design*. New York: Wiley, 1982, p. 127, Fig. 4.9.

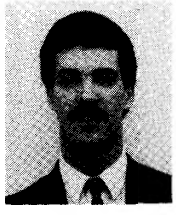

Joseph A. Shaw (S'85–M'87) was born in Bozeman, MT, on June 7, 1962. He received the B.S. degree (*cum laude*) from the University of Alaska, Fairbanks, in 1987, and the M.S. degree, both in Electrical engineering, from the University of Utah, Salt Lake City, in 1989.

Since 1989 he has been employed at the Wave Propagation Laboratory of the National Oceanic and Atmospheric Adminstration in Boulder, CO. During this time he has worked on computer modeling and hardware development for microwave and infrared radiometric techniques for ground-based atmospheric remote sensing and satellite communications propagation studies.

Mr. Shaw is a member of Phi Kappa Phi, the IEEE Antennas and Propagation Society, and the Society of Photo-Optical Instrumentation Engineers.

Carl H. Durney (S'60–M'64–SM'80) was born in Blackfoot, ID, on April 22, 1931. He received the B.S. degree in electrical engineering from Utah State University, Logan, in 1958, and the M.S. and Ph.D. degrees in electrical engineering from the University of Utah, Salt Lake City, in 1961 and 1964, respectively.

From 1958 to 1959, he was employed as an Associate Research Engineer with the Boeing Airplane Company, Seattle, WA, where he investigated the use of delay lines in control systems. He has been with the University of Utah since 1963, when he was appointed to be Assistant Research Professor of Electrical Engineering. From 1965 to 1966, he was employed at the Bell Telephone Laboratories, Holmdel, NJ, while on leave from the University of Utah. During this time, he worked in the area of microwave avalanche diode oscillators. In 1971, he was engaged in study and research involving microwave biological effects at the University of Washington while on leave from the University of Utah. From 1977 to 1982, he was chairman of the Department of Electrical Engineering at the University of Utah. While on sabbatical leave from the University of Utah during the 1983–1984 academic year, he was Visiting Professor at the Massachusetts Institute of Technology, Cambridge, where he was engaged in research in nuclear magnetic resonance imaging and hyperthermia for cancer therapy. He is presently Professor of Electrical Engineering and Professor of Bioengineering at the University of Utah where he is teaching and doing research in electromagnetics, engineering pedagogy, electromagnetic biological effects, and medical applications of electromagnetics.

Dr. Durney is a member of the Bioelectromagnetics Society, Commission B of URSI (International Union of Radio Science), Sigma Tau, Phi Kappa Phi, Sigma Pi Sigma, Eta Kappa Nu, the American Society for Engineering Education, and the North American Hyperthermia Group. He served as Vice President (1980–1981) and President (1981–1982) of the Bioelectromagnetic Society, as a member (1979–1988) and Chairman (1983–1984) of the IEEE Committee on Man and Radiation (COMAR), as

the American National Standards Institute C95 Subcommittee IV on Radiation Level and/or Tolerances with Respect to Personnel (1973–1988), as a member of the editorial board of the IEEE TRANSACTIONS ON MICROWAVE THEORY AND TECHNIQUES (1977–present), and as a member of the editorial board of *Magnetic Resonance Imaging* (1982–present). In 1983, he served as co-editor for a special issue of the *Journal of Microwave Power* on "Electromagnetic techniques in medical diagnosis and imaging." In 1980, he received the Distinguished Research Award from the University of Utah, and the Outstanding Teaching Award, College of Engineering, University of Utah. In 1982, he received the American Society for Engineering Education Western Electric Fund Award for excellence in teaching, and the Utah Section IEEE Technical Achievement Award. He was named a College of Engineering Distinguished Alumnus by Utah State University in 1983. In 1990, he was named the Utah Engineering Educator of the Year by the Utah Engineering Council.

Douglas A. Christensen (M'69) received the B.S.E.E. degree from Brigham Young University, Provo, UT, in 1962, the M.S. degree from Stanford University, Stanford, CA, in 1963, and the Ph.D. degree from the University of Utah, Salt Lake City, in 1967.

He has been a faculty member at the University of Utah since 1971. He currently holds a joint appointment as Professor of Electrical Engineering and Professor of Bioengineering. His major research interests are in area of waves in biological sensing, such as optical biosensors, fluorescent waveguiding immunosensors, numerical modeling of optical waveguides and near-field optical effects, and ultrasonic bioinstrumentation. He is the author of the textbook *Ultrasonic Bioinstrumentation* (New York: Wiley, 1988).